ELSEVIER

Journal of Crystal Growth 217 (2000) 332–343

JOURNAL OF CRYSTAL GROWTH

www.elsevier.nl/locate/jcrysgro

Banded spherulitic growth in a liquid crystal

Jeffrey L. Hutter*, John Bechhoefer

Department of Physics, Simon Fraser University, Burnaby, British Columbia, Canada V5A 1S6

Received 29 September 1999; accepted 18 April 2000
Communicated by M.E. Glicksman

Abstract

Spherulitic growth produces radial arrays of polycrystalline aggregates in a wide variety of materials, ranging from pure elements to macromolecules. Despite more than a century of study, a generally accepted theory of spherulitic growth is lacking; indeed, the existence of a common mechanism is debated. One commonly seen subset of this growth morphology — banded spherulites — exhibits bands concentric about the spherulite centers. These bands have been well characterized in polymer spherulites, but remain poorly understood. Comparisons of such bands in a diverse variety of materials will help establish a general mechanism for their formation. Here we present a detailed optical and atomic-force microscopy study of banding in a liquid crystalline material.

PACS: 61.50.Jr; 64.70.Md; 81.30.Fb

Keywords: Solidification; Crystal morphology; Spherulite; Banded spherulite

1. Introduction

Spherulites consist of radially oriented microcrystals arranged at noncrystallographic angles within a spherical envelope. This growth form is most familiar in polymers, where spherulites are the typical crystallization mode [1–6] (although not all polymer solids are crystalline). However, spherulites have also been investigated in materials as dissimilar as elemental selenium [7–9], low molecular weight systems with polymeric impurities [10], organic materials [11,12], biological molecules [2], mineral aggregates (references in minerals date to Refs. [13–15]), and liquid crystals [16–18]. The presence of spherulites influences the mechanical properties of commercial materials. For example, the carbon in cast iron often forms spherulites [19], resulting in a metal which is much less brittle than cast iron in which the carbon forms graphite sheets. Here, the formation of spherulites is desirable. In biological sciences, where large single crystals of proteins are required for X-ray structural studies, spherulites are a common "failure mode" [2,20]. Clearly, an understanding of when spherulites form would benefit many areas of science and technology.

Despite this importance — and a century of study [13] — there is no generally accepted theory of spherulitic growth. Even more mysterious is the origin of the concentric bands which often accompany spherulitic growth. Although the nature of

* Corresponding author. Present address: Department of Physics and Astronomy, University of Western Ontario, London, Ont., Canada N6A 3K7. Tel.: +1-519-661-2111, ext. 86719; fax: +519-661-2033.

E-mail address: jhutter@julian.uwo.ca (J.L. Hutter).

0022-0248/00/$ - see front matter
PII: S0022-0248(00)00479-6

Table 1
Properties of 10OCB

Quantity	Symbol	Value	Units	Ref.
Chemical name	—	4–cyano–4′–decyloxybiphenyl	—	—
Formula	—	$C_{23}H_{29}ON$	—	—
Molecular weight	—	335.49	g/mol	—
Chemical abstracts no.	—	70247-25-5	—	—
Density (solid)	ρ	1.098	g/cm^3	[28]
Viscosity (SmA)[a]	η	$\sim$0.2–1	Pa s	
Thermal diffusivity (SmA)[b]	D_h	$\sim 10^{-3}$	cm^2/s	
Specific heat (SmA)	c_p	$\sim$2	J/g °C	[31]
Latent heat of solidification	L	115	J/g	[31]
Solid–smectic A transition[c]	$T_{\mathrm{K-SmA}}$	59.5	°C	
Smectic A–isotropic transition[c]	$T_{\mathrm{SmA-I}}$	84	°C	

[a] Viscosity data for a similar compound, 8OCB, have been measured as a function of temperature by K. Negita [29].
[b] Thermal diffusivities of similar compounds are given by U. Zammit et al. [30].
[c] BDH Limited, Broom Road, Poole, BH12 4NN, England.

these bands is known in some systems (for instance, in polymers the bands are associated with a periodic rotation of the optical axis along the spherulite radius [1–3,21,22]), the mechanism responsible for their formation remains elusive.

The striking similarity of spherulites in diverse systems suggests a corresponding similarity in growth mechanisms.[1] If a common mechanism exists, comparison of spherulitic growth in dissimilar materials can identify those features that are fundamental to such a mechanism. Here, we compare and contrast both banded and unbanded spherulites solidified from a liquid crystalline material with those grown from other systems. In the following section, we motivate the choice of material studied and describe the experimental techniques used. In Section 3, we discuss the general features of the spherulites formed and compare with other spherulitic systems. Section 4 presents studies of the growth dynamics. We conclude with a discussion of implications for the general mechanism of spherulitic growth.

2. Experimental procedure

We chose to study spherulitic solidification of the liquid crystalline material 4–cyano–4′–decyloxybiphenyl (10OCB). In previous publications [18,25–27], we described the wide variety of growth morphologies exhibited by 10OCB, and showed that transitions between these morphologies occur at well-defined growth temperatures and are accompanied by sharp changes in growth properties such as the growth velocity and front shape. This system is experimentally convenient: it is available in quite pure form,[2] it is chemically stable, and its properties are well known (see Table 1).

The "intermediate" properties of liquid crystals result in natural growth velocities between those of simple molecular systems, which often grow too quickly to allow detailed observations, and those of macromolecular systems, which typically freeze at inconveniently slow rates [32]. Spherulitic growth in 10OCB occurs at approximately room temperature and with velocities of the order of 100 μm/s.

[1] Despite the striking simularities between spherulites in diverse systems, proposed models of spherulite banding are often specific to polymers, implying that the phenomenon may be material specific. See Refs. [23,24].

[2] The 10OCB is nominally pure, but does contain 0.15% water at the saturation limit. Samples prepared by heating under vacuum to remove volatile impurities, as well as samples doped with $\sim$2 mol% C_2Cl_6, showed the same solidification behavior, suggesting that the morphologies are not impurity driven.

The samples consisted of thin (10 μm) layers of 10OCB sandwiched between two glass plates. We used thin (~170 μm) plates to ensure rapid cooling to the desired temperature. A typical solidification experiment begins by melting the sample into the isotropic phase on a hot plate. The sample is then quickly transferred to a computer-controlled hot stage[3] set to the desired undercooling. The sample quickly enters a supercooled smectic phase, after which the solid phase nucleates. Spherulitic growth was observed for temperatures less than approximately 40°C, corresponding to undercoolings greater than approximately 20°C.

We studied the solidification front using optical microscopy,[4] recording the images with a video camera[5] and frame grabber.[6] The front location and shape were determined by applying a threshold to the images and selecting the pixels dividing the darker solidified material from the melt.[7] We tracked the motion of this front to determine its velocity.

We also used optical microscopy to observe spherulitic growth in directional solidification [33]. In a directional solidification experiment, the sample is driven at a constant velocity through a temperature gradient produced by a narrow gap between two temperature stages. The temperature difference is set so that the solidification front is visible within the gap. After an initial transient when the sample motion begins, the front approaches a steady state which is stationary within the lab frame, allowing the front to be studied for a period of time set by the sample dimensions.

Finally, the microstructures of the samples were studied using an atomic-force microscope (AFM)[8] after solidification was complete. The sandwich cells described above could be pried apart, usually resulting in cleavage along one of the plates. Such cleavage did not alter the visual appearance of the spherulites; in addition, AFM images of samples prepared without a top plate exhibited similar topography.

3. Classical spherulitic growth in 10OCB

In this section, we examine the properties of 10OCB spherulites and show that they exhibit features associated with spherulites in other systems.

3.1. Spherulites are round

Observations of spherulitic growth usually reveal that the growing solid phase defines a slowly expanding spherical envelope within a viscous fluid. One qualitative difference between the system studied here and more familiar spherulite forming systems is that growth proceeds from a smectic liquid crystalline phase, rather than from an isotropic melt. Not surprisingly, solidification from an ordered phase can result in anisotropic growth. For most of our experiments, we treated the glass plates with an organosilane[9] to impose homeotropic anchoring with the smectic layers parallel to the surfaces, thus creating a uniform, defect-free sample. This removes the anisotropy in the sample plane and results in round spherulites.

Experiments performed with cells treated for planar anchoring (i.e., with smectic layers perpendicular to the surfaces) resulted in spherulites that differed only in the growth anisotropy: the growth was slowest in the anchoring direction, resulting in oval "spherulites" with an aspect ratio of ~0.9, as shown in Fig. 1. We achieved this anchoring by slowly (~1 mm/min) drawing the plates from a beaker containing a polyimide solution to obtain a thin polymer layer with molecules aligned in the drawing direction, baking at 150°C to remove the solvent, and gently rubbing with a fine cloth in

[3] HS1-i Microscope Hot Stage and Temperature Controller, Instec, Inc., Boulder, CO 80306.

[4] Olympus BH-2 Olympus Optical Company, Lmt., Tokyo, Japan.

[5] Pulnix TM-7CN, Pulnix America, Inc., Sunnyvale, CA 94086.

[6] Scion LG-3, Scion Corporation, Frederick, MD 21701.

[7] Image processing was performed using the software package NIH Image, v. 1.61. National Institute of Health, Division of Computer Research and Technology, USA The procedure is described in more detail in Ref. [27].

[8] Universal AFM/STM. Park Scientific Instruments, Sunnyvale, CA 94089-1304.

[9] ZLI 2510, E. Merck, Darmstadt, Germany.

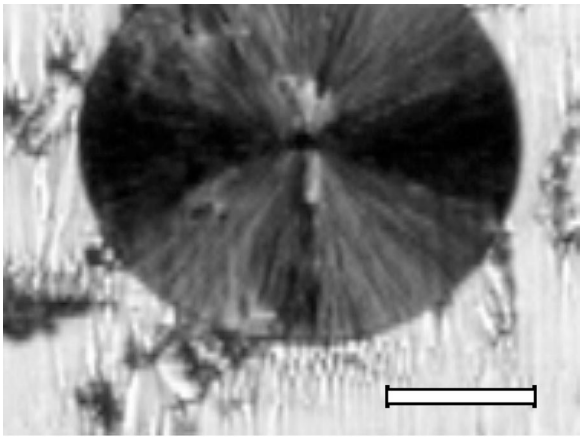

Fig. 1. Oval spherulite in a planar-anchored sample. The scale bar measures 100 μm.

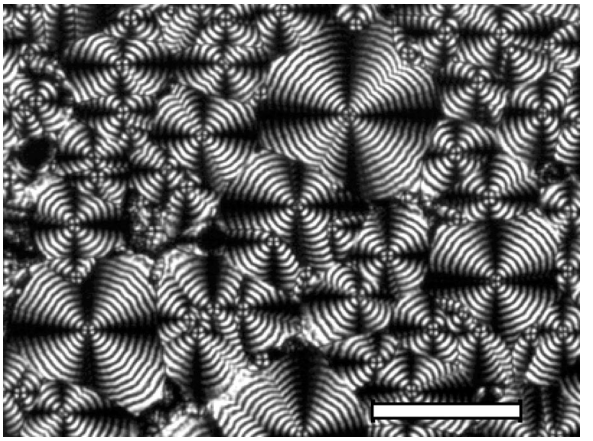

Fig. 2. Collection of spherulitic domains viewed through crossed polarizers. Note the characteristic "Maltese cross" pattern, indicating a 360° rotation in crystal orientation about the nuclei, and the concentric bands due to rotation of the optic axes about this radial direction (by 180° for each band). The scale bar represents 25 μm.

the drawing direction. The resulting plates force the liquid crystal molecules to align along the drawing direction, resulting in smectic planes perpendicular to this direction. Since this anchoring causes faster growth in the direction of the smectic planes, it is possible that molecules aligned tangentially to the spherulite front are more easily incorporated into microcrystals. Other than the oval shape, there is no obvious difference between spherulites formed in planar and homeotropic anchoring. In the remainder of this paper, we consider homeotropic anchoring only.

3.2. Spherulites consist of radial arrays of microcrystals

Aside from the spherical (or circular, in two dimensions) shape of spherulites, the classical characteristic of this growth morphology is a radial orientation of microcrystals. The cause of this orientation is unknown and may be system-dependent. One way to achieve such a noncrystallographic radial alignment is to impose a pressure between neighboring crystallites. In polymers, which form ribbon-like lamellae, Bassett, Keller, and Misuhashi [6,34,35] have proposed that this pressure is an entropic pressure due to dangling polymer chains in the gap between lamellae. Such a model cannot apply to materials formed from smaller molecules. In such cases, Tiller [36] has suggested that the splay is due to viscous flow of the melt induced by the density change during solidification. Flow through the narrow channels separating adjacent needle crystals (towards the center of the spherulite, if the solid is more dense than the liquid) will generate a pressure according to the Hagen–Poiseuille equation.

Although the microscopic mechanism of splay is quite different for the two cases discussed above, both predict a radial arrangement of initially parallel crystals caused by crystal bending (or breaking, if the mechanical strain is great enough). Since this requires the orientation of the crystals to vary with angular position about the spherulite center, spherulites often exhibit a "Maltese cross" pattern when viewed through crossed-polarizers [3]. As shown in Fig. 2, this pattern is observed for 10OCB spherulites. Here, dark bands concentric with the nucleus are also seen. The AFM allows us to image the radial orientation directly (cf. Fig. 8 below).

There is good evidence for a density change and resultant flow during the growth of 10OCB spherulites. We estimated the change in density by measuring the change in size of small droplets (200–800 μm in diameter) sandwiched between glass plates held 25 μm apart as they are solidified. Since the solid phase is denser than the smectic A,

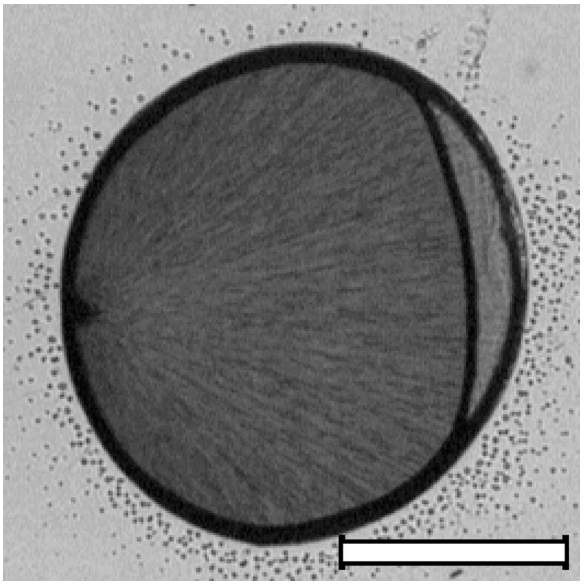

Fig. 3. Density change during solidification of a small droplet of 10OCB at an undercooling of 30 °C between glass plates 25 μm apart. The density change causes the droplet to shrink. The original shape is still visible because of a thin (estimated from the depth of focus to be ~ 1 μm) film of material which freezes to the glass plates. The scale bar spans 200 μm.

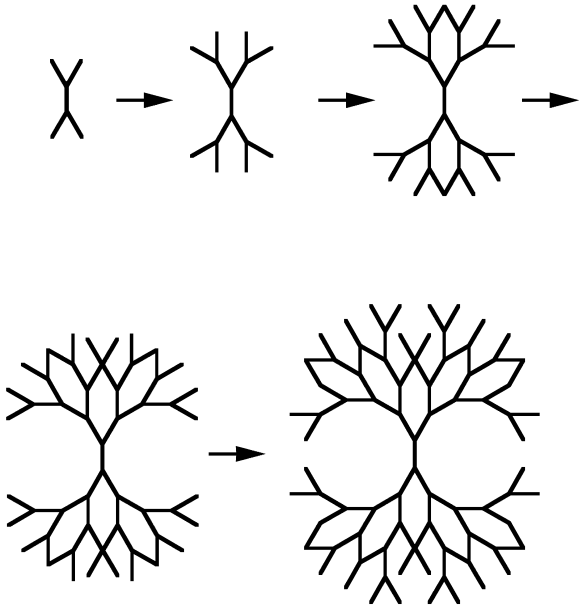

Fig. 4. Evolution of the "sheaf-like" spherulite nucleus.

the drops shrink during solidification, as shown in Fig. 3. Note that the solid drop is not perfectly circular because the solid phase does not usually nucleate at the center. This results in increased flow from the regions further from the nucleus. We found that the density change is approximately 10% for spherulitic growth, although the thin film of material left on the plates as the droplet shrinks makes a precise estimate difficult. We will see that the spherulitic morphology is not compact on the microscopic scale. Thus, this density change must be regarded as an average value over the spherulite domain, and is not representative of the intrinsic volume change for the phase transition.

3.3. Spherulite nuclei

A model of microcrystals radiating from a central nucleus requires a defect at the origin. High-resolution studies of spherulite nuclei reveal a pattern known in the literature as a "sheaf of wheat" morphology, due to its resemblance to a tied sheaf of wheat. The standard explanation [14,37] is that the spherulite initially nucleates as a single needle, from which new needles branch. As the spherulite gets larger, the needles are forced into a radial orientation. If there is a maximum branching angle and/or minimum radius of curvature, the result is an asymmetric nucleus with two cavities which are inaccessible to crystals branching from the original nucleus, and a defect line where needles from opposite ends of the nucleus meet. This process is shown schematically in Fig. 4.

10OCB spherulites also exhibit this sheaf form, as shown by the AFM images in Fig. 5, which are also complicated by concentric bands. Occasionally nuclei are seen with a spiral banded structure, rather than the sheaf form (Fig. 6). These may result from nucleation at heterogeneous sites such as dust particles.

3.4. Banded spherulites

Most of the spherulites discussed in this paper are banded. Banding in spherulites is generally accepted to be due to a birefringent effect [1–3,21,22]. Observations suggest that the optical

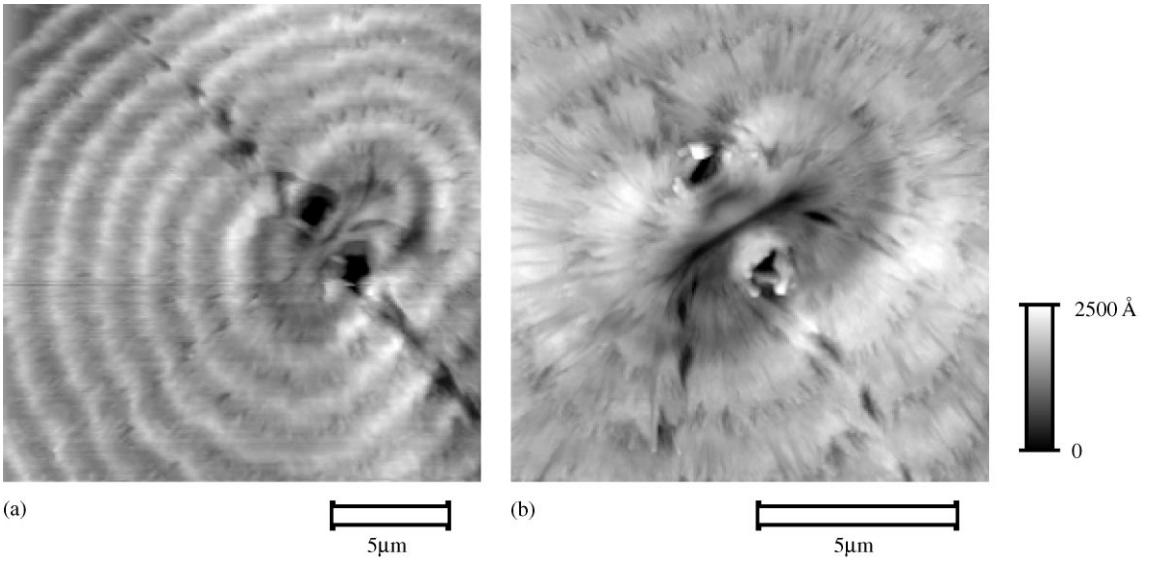

Fig. 5. AFM micrographs of spherulite nuclei with sheaf structures.

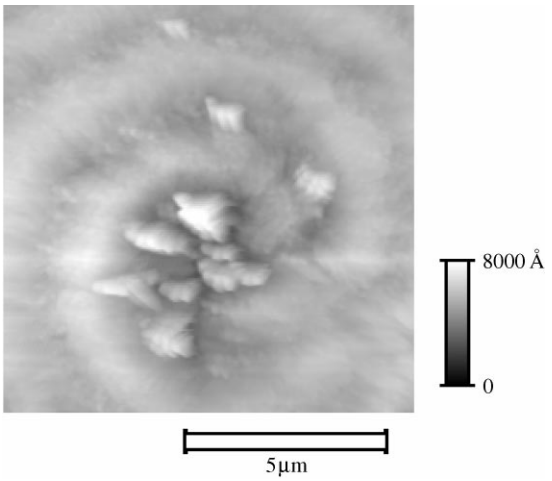

Fig. 6. Spherulite nucleus with a spiral structure.

axis of the crystallites follows a helical path about the spherulite radius. When viewed through crossed polarizers, dark bands are seen at radii where the optical axis lies along the line of sight. This hypothesis is supported by an apparent shift in band position when the sample is tilted, thus rotating the optic axis about the tilt axis.

Twist in the unit cell orientation has been confirmed in some systems by electron microscopy [1,2,6,38,39], microbeam X-ray diffraction [40], and micro-Raman spectroscopy [41]. The existence of this twist can be due either to a continuous twist of individual crystallites or to a dependence on radius of the average orientation of (untwisted) crystals. The second possibility is generally believed more likely [2,39]. However, some electron micrographs of polymer spherulites indicate that the lamellae are flat throughout most of the band, with the twist occurring over a relatively short distance [2,6,39].

Fig. 7 shows an optical micrograph of a portion of a large spherulite. The center of the spherulite is far outside the field of view, resulting in bands that are nearly planar on the scale of the image. Note that sharp phase shifts occur along the bands, resulting in lines perpendicular to the bands separating regions of coherent banding. AFM images (Fig. 8) show that these phase shifts are discontinuous at the scale of the microcrystals which make up the spherulite.

If we view spherulites illuminated by unpolarized light through a single polarizer, we find that the band contrast is greatest when the polarizer is aligned parallel to the bands. When the polarizer passes light polarized perpendicularly to the bands, the contrast is so weak that the bands cannot be

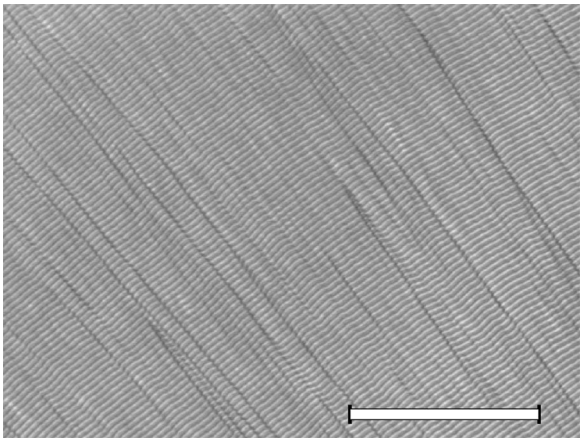

Fig. 7. Optical micrograph of a domain of banded spherulitic growth. Note that the structure is divided into sub-domains separated by phase shifts in the bands. This sample was solidified at an undercooling of about 40°C, resulting in a band spacing of 1.7 μm. The scale bar measures 50 μm.

distinguished. This indicates that the contrast depends on an attenuation (by scattering, since absorption is negligible in the visible for 10OCB) of the component of light polarized along the bands. This supports the picture of an optical axis that rotates about the spherulite radius (i.e., about the long axes of the microcrystals) — such a rotation does not alter the refractive index in the radial direction, so that light polarized in the radial direction encounters no variation in refractive index and produces no contrast.

We used the AFM and scanning electron microscope (SEM) to study the structure of the bands on length scales of the band spacing and smaller. As seen in Fig. 8, the bands are composed of individual needle crystals approximately 600 Å wide. Different banded domains are separated by discontinuities in the band phase, as discussed earlier. The apparent separation of bands *within* a single domain is not as readily understood.

Fig. 8b shows many of the needle crystals ending at well-defined band edges. Fig. 8a, however, does not show such clear boundaries and contains examples of needles which extend across more than one band. In neither case is the AFM resolution sharp enough to reveal a twist in the needle crystals. It is important to realize that the image measured by

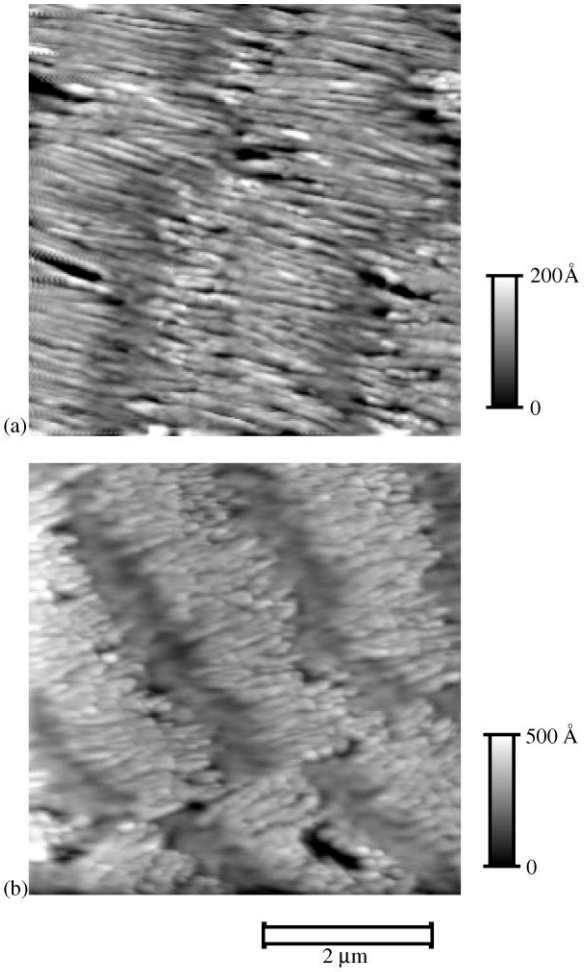

Fig. 8. Atomic-force micrographs of spherulitic bands. The samples were grown between glass plates, which were subsequently pried apart. The bands are composed of radially oriented needles with lengths on the order of the band spacing. (a) Spherulite grown at $\Delta T = 25°C$. (b) Spherulite grown at $\Delta T = 32°C$. Note the sharp change in band phase.

the AFM is a map of the sample height required to maintain a constant deflection force on the cantilever. As such, the image contains both topographical and mechanical information [42]. For instance, a soft region of the sample is difficult to distinguish from a depression in the surface. The fact that bands can be seen in these images indicates that they are associated with a modulation in either sample height or stiffness.

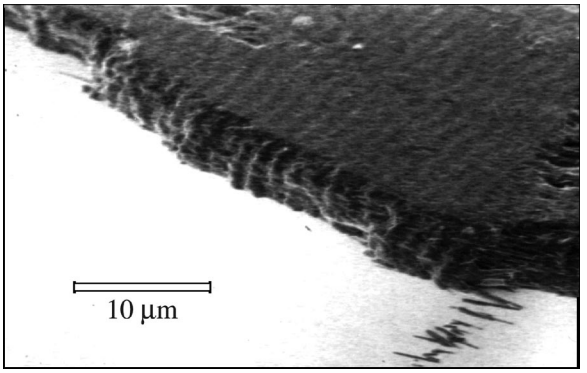

Fig. 9. Scanning electron microscope image of a banded spherulite. The image shows a fractured spherulite with bands visible on both the surface and fractured edge. The growth direction was to the lower left.

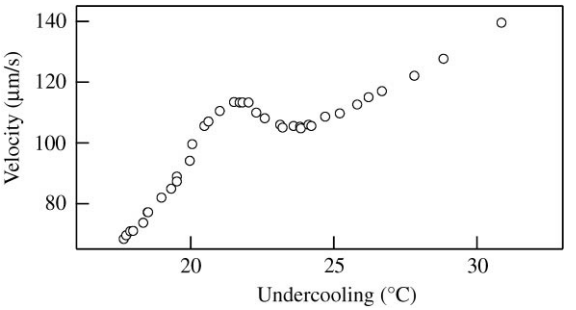

Fig. 10. Growth velocity as a function of undercooling in the spherulitic regime. The transition between unbanded and banded spherulites occurs at $\sim 22^{\circ}$C, with banded spherulites at larger undercoolings.

A modulation in sample stiffness could arise from a twist in the average orientation of microcrystals: anisotropy in the mechanical properties of the needle crystals would result in a variation in sample stiffness across each band. It is perhaps more likely that the bands seen with the AFM represent a real surface buckling that occurs after cleavage to relieve stresses. Below, we present evidence for the existence of stress in 10OCB spherulites.

In order to examine the bands inside the domains, we used the SEM to image freshly fractured spherulite edges. We prepared the spherulites for the SEM study on a highly doped silicon wafer to provide a conducting substrate. Both the silicon and glass cover plate were treated for homeotropic anchoring. After removal of the glass plate, the spherulite was fractured to provide fresh surfaces revealing the interior banding structure. An example is shown in Fig. 9. To avoid sample damage and charging effects we accelerated the electron beam through a relatively small potential (1 kV) and carefully adjusted the current so that the incident flux was balanced by electrons emitted from the sample. The bands are clearly visible throughout the sample bulk. This image also shows some isolated needle crystals that have detached from the spherulite. As with the AFM images, these crystals have lengths of the order of a band spacing.

4. Spherulite growth

Having established that the 10OCB spherulites show all of the features seen in spherulites of other materials, we turn our attention to the variation of these features with growth conditions.

4.1. Growth velocity and band spacing

In previous publications, we examined transitions between 10OCB growth morphologies as a function of undercooling. Unlike the other transitions studied, the unbanded to banded transition is not accompanied by a sharp change in growth velocity, although as shown in Fig. 10, the velocity curve does undergo an unusual excursion in this vicinity (at $\sim 22^{\circ}$C). We found that other quantities such as the band spacing and measures of fluctuations (for instance the band coherence length) do appear to diverge at the transition.

We also measured the band spacing of spherulites grown by directional solidification. The undercoolings for these domains were not measured (accurate measurement of undercooling in directional solidification is difficult), but the isothermal and directional solidification results can be compared on a plot of band spacing vs. growth velocity. Fig. 11 compares the band spacing for isothermal growth at a variety of sample thicknesses and directional solidification in an imposed temperature gradient.

4.2. Dependence of bands on local features

The fact that the band spacing has the same dependence on growth velocity for differing conditions implies that the details of diffusion fields and other long-range properties are unimportant to the banding mechanism. This conclusion is further strengthened by observations of growth in very small domains. Examples are shown in Fig. 12. The large droplet in Fig. 12a shows a spherulite with a nucleation point at the top edge. The banded domain was able to propagate to the lower section of the droplet through an isthmus only a few band spacings wide. Fig. 12b shows several instances of banding in domains whose total extent is only a few band spacing. These results indicate that the banding mechanism depends only on properties on the length scale of the banding.

Occasionally, a growing spherulite would encounter an air bubble within the sample. The result, as shown in Fig. 13, is a domain which is unperturbed save near the end of the bubble furthest from the spherulite origin, where the bands bend around the far side of the bubble (this effect has also been discussed in polymeric spherulites [43]). This again demonstrates the insensitivity to all but very local perturbations.

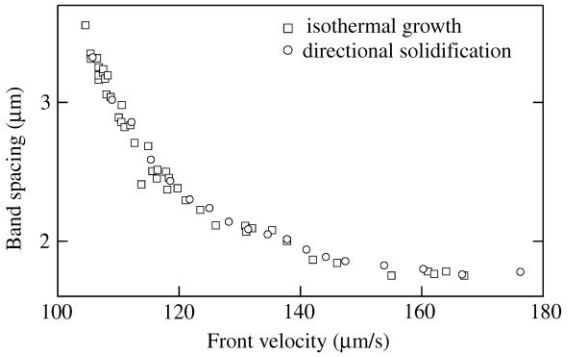

Fig. 11. Spherulite band spacing as a function of growth velocity. Note that both sets of data — isothermal growth with sample thicknesses ranging from 10 to 50 μm and directional solidification with an applied gradient of 50°C/mm — fall onto a single curve.

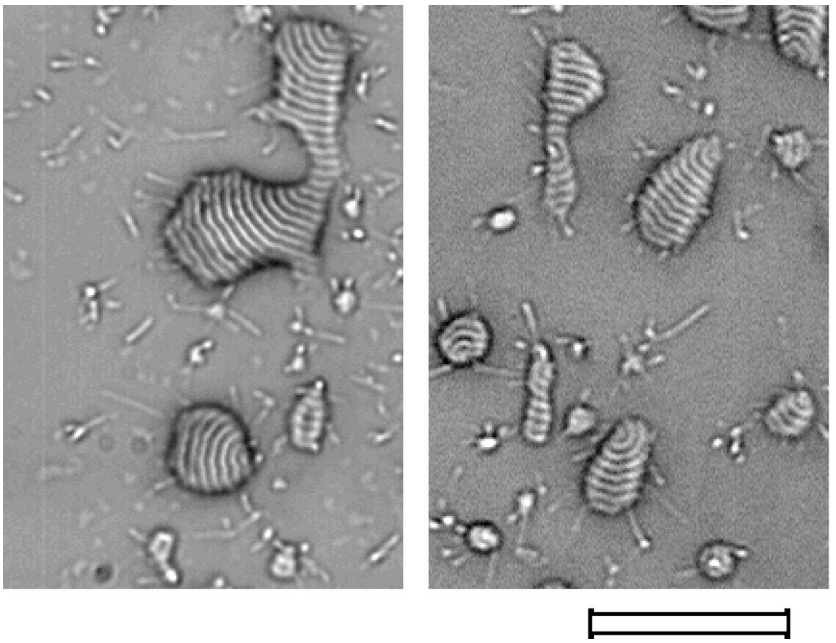

Fig. 12. Spherulitic growth in small and irregular droplets. The bands are able to propagate through features with sizes of the order of the band spacing. In addition, banding is seen in droplets only two bands across. The scale bar of 25 μm applies to both images.

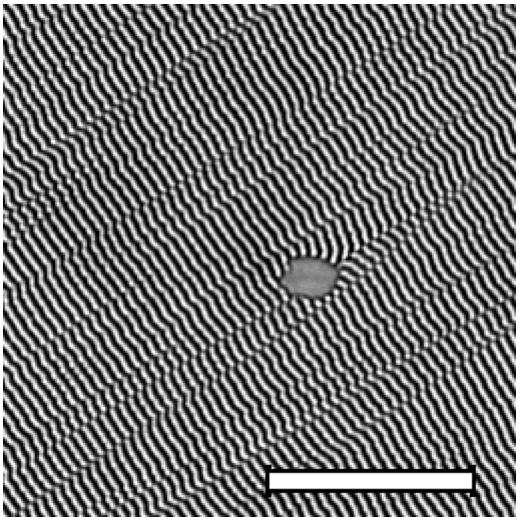

Fig. 13. Spherulitic growth around an air bubble. Note that the bands are unperturbed until forced to fill in the region behind the bubble. Growth was to the upper right and the scale bar spans 25 μm.

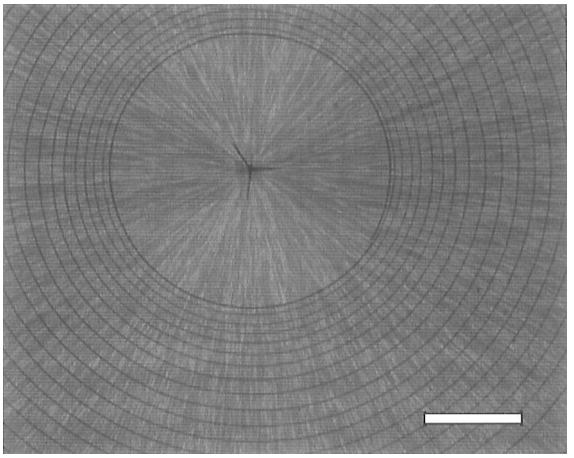

Fig. 14. Fracture of banded spherulites. Within a period of hours, 10OCB spherulites often crack along the bands. Radial cracks originating at the nucleus are also seen. A scale bar of 200 μm is shown.

4.3. High-speed observations

High-resolution real-time observations of banded spherulite growth would aid in the development of a growth mechanism. The growth of 10OCB is too rapid to allow AFM investigations. Instead, we studied the growth using high-speed (up to 5000 frames/s) video microscopy. One of the objectives of this approach was to determine whether or not the front velocity oscillates with the banding. Such an oscillation would be incompatible with a continuous twist of microcrystals, for instance. While some of our observations did reveal such an oscillation, we saw no clear trend with undercooling (indeed, some runs showed no oscillation at all). Thus, the apparent oscillation was most likely an effect of the band contrast — advance of the front is more difficult to see during phases when the band has low contrast with the surrounding melt.

4.4. Spherulite stability

Although banded spherulites are stable enough to allow them to be studied, 10OCB spherulites are not stable at room temperature. This is not surprising since they are grown far from equilibrium. In fact, spherulites of some materials can break up with explosive force [4]. Our 10OCB spherulites often fracture concentrically along the bands (see Fig. 14) within a period of hours, indicating a built-in mechanical stress.

Over a period of several days, the bands disappear completely. This process can be accelerated by heating the spherulites. Annealing at a few degrees below the melting point causes the bands to disappear in a matter of moments. A well-defined front associated with this change can be seen in Fig. 15a. In this example the "unbanding" front had a velocity of ~ 10 μm/s. Examination of the microstructure after the destruction of the bands, Fig. 15b, shows that a change in morphology has occurred: the microcrystals have become much larger and all remnants of the band ordering have vanished (compare with Fig. 8). X-ray diffraction shows that the crystal structure, or at least orientation, has also changed.

5. Conclusions

Spherulitic growth is a little-understood growth morphology frequently seen in a diverse range of

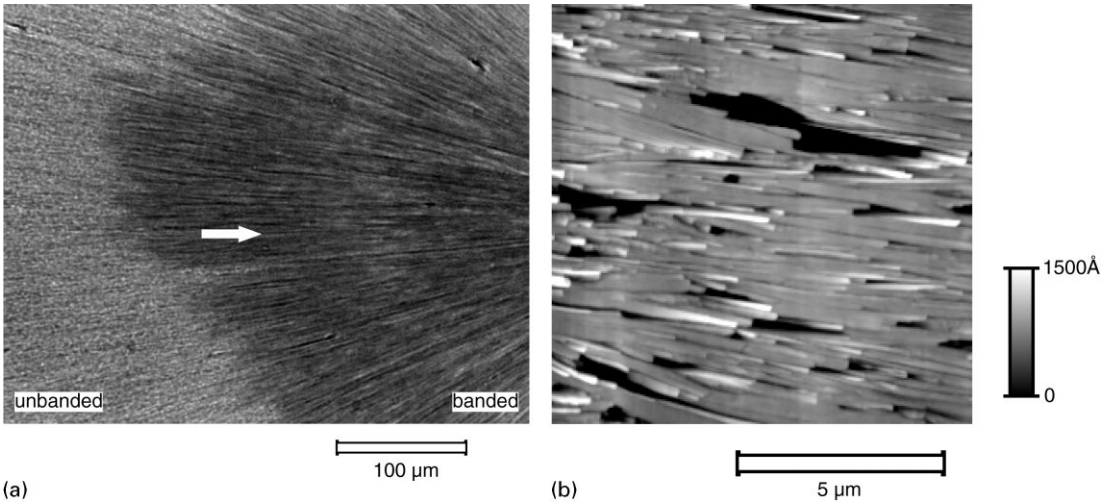

Fig. 15. Annealing of banded spherulites. (a) "Unbanding front" sweeping toward the center of the spherulite. This image was taken after a few minutes of annealing $\sim 5^{\circ}$C below the melting point. (b) AFM micrograph of a spherulite after the front in (a) has passed. Note that the bands are no longer present.

materials. The similarity of spherulites in these differing materials suggests a common growth mechanism. We have studied spherulitic growth in a liquid crystalline material with the goals of identifying the features shared by other spherulites and studying the growth kinetics in an experimentally convenient system.

Our spherulites, in common with those seen in other materials, are composed of radially oriented microcrystals originating from a sheaf-like nucleus and growing with a front that is smooth on a scale larger than the individual crystals.

Our observations of banded spherulites grown in temperature gradients and in small and irregular domains show that only properties very near the growth front are important — sample conditions only a few band wavelengths from the front are not important. This dependence on local properties gives hope that a simple model may be found. Other hints are provided by the evidence (such as the diverging band spacing shown in Fig. 11) that the transition to the banded regime is analogous to a second-order phase transition and occurs in a region where the front velocity is a decreasing function of undercooling (Fig. 10) [26,27].

Many careful microscopic studies of spherulitic growth in a variety of materials exist in the literature. Further studies of their growth kinetics, particularly near the transition to the banded regime, would be of great use in developing a universal theory of spherulitic growth.

Acknowledgements

This work was funded by NSERC (Canada). The authors would like to thank Tom Pinnington and Robin Coope for the SEM micrograph shown in Fig. 9, Tom Mason for the use of a high-speed video camera, and Mike Degen and Matthew Case for help in analyzing the images.

References

[1] P.J. Phillips, Rep. Prog. Phys. 53 (1990) 549.
[2] P.J. Phillips, Spherulitic crystallization in macromolecules, in: D.T.J. Hurle (Ed.), Handbook of Crystal Growth, Vol. 2, Elsevier, Amsterdam, 1993 (Chapter 18).
[3] A. Keller, J. Polym. Sci. 17 (1955) 291.
[4] H.D. Keith, F.J. Padden Jr., J. Appl. Phys. 34 (1963) 2409.
[5] G. Schuur, J. Polym. Sci. 11 (1953) 385.
[6] D.C. Bassett, CRC Crit. Rev. Solid State Mater. Sci. 12 (1986) 97.
[7] G. Ryschenkow, G. Faivre, J. Crystal Growth 87 (1988) 221.

[8] J. Bisault, G. Ryschenkow, G. Faivre, J. Crystal Growth 110 (1991) 889.
[9] M. Mohan, A.K. Singh, Philos. Mag. B 67 (1993) 705.
[10] R.R. Lagasse, J. Crystal Growth 140 (1994) 370.
[11] J.H. Magill, D.J. Plazek, J. Chem. Phys. 46 (1967) 3757.
[12] F.P. Price, A. Keith Fritzsche, J. Phys. Chem. 77 (1973) 396.
[13] P. Iddings, Am. J. Sci. 33 (1887) 36.
[14] H.W. Morse, J.D.H. Donnay, Am. Mineral. 21 (1936) 391.
[15] P.J. Heaney, A.M. Davis, Science 269 (1995) 1562.
[16] F. Rinne, Trans. Faraday Soc. 29 (1933) 1016.
[17] S.C. Jain, S.A. Agnihotry, V.G. Bhide, Mol. Cryst. Liq. Cryst. 88 (1982) 281.
[18] J.L. Hutter, J. Bechhoefer, Physica A 239 (1997) 103.
[19] B. Miao, D.O. Northwood, W. Bian, K. Fang, M.H. Fan, J. Mater. Sci. 29 (1994) 255.
[20] A. Ducruix, R. Giegé (Eds.), Crystallization of Nucleic Acids and Proteins: A Practical Approach, Oxford University Press, Oxford, 1992.
[21] H.D. Keith, F.J. Padden Jr., J. Polym. Sci. 31 (1958) 415.
[22] A. Keller, J. Polym. Sci. 39 (1959) 151.
[23] H.D. Keith, F.J. Padden Jr., Polymer 25 (1984) 28.
[24] A.J. Owen, Polymer 38 (1997) 3705.
[25] J. Bechhoefer, J.L. Hutter, Physica A 249 (1998) 82.
[26] J.L. Hutter, J. Bechhoefer, Phys. Rev. Lett. 79 (1997) 4022.
[27] J.L. Hutter, J. Bechhoefer, Phys. Rev. E 59 (1999) 4342.
[28] S. Gupta, S. Paul, Indian J. Phys. 68A (1994) 465.
[29] K. Negita, Int. J. Mod. Phys. B 13 (1999) 2005.
[30] U. Zammit, M. Marinelli, R. Pizzoferrato, F. Scudieri, S. Martellucci, Phys. Rev. A 41 (1990) 1153.
[31] J.L. Hutter, Solidification of a liquid crystal: morphologies and transitions, Ph.D. Thesis, Simon Fraser University, Burnaby, BC, Canada, 1997.
[32] J. Bechhoefer, Nonequilibrium phenomena in liquid crystals, in: P.E. Cladis, P. Palffy-Muhoray (Eds.), Spatio-Temporal Patterns in Nonequilibrium Complex Systems, Santa Fe Institute: Studies in the Sciences of Complexity, 21, Addison-Wesley, Reading, MA, 1994, pp. 107–122.
[33] J.D. Hunt, K.A. Jackson, H. Brown, Rev. Sci. Instr. 37 (1996) 805.
[34] D.C. Bassett, A. Keller, S. Mitsuhashi, J. Polym. Sci. A 1 (1963) 763.
[35] D.C. Bassett, Philos. Trans. Roy. Soc. London A 348 (1994) 29.
[36] W.A. Tiller, The Science of Crystallization: Microscopic Interfacial Phenomena, Cambridge University Press, Cambridge, 1991, pp. 342–347.
[37] A. Keller, J. Polym. Sci. 17 (1955) 447.
[38] D.C. Bassett, A.M. Hodge, Polymer 19 (1978) 469.
[39] D.C. Bassett, A.M. Hodge, Proc. Roy. Soc. London A 377 (1981) 61.
[40] Y. Fujiwara, J. Appl. Polym. Sci. 4 (1990) 10.
[41] H. Tanaka, T. Ikeda, T. Nishi, Appl. Phys. Lett. 48 (1986) 393.
[42] N.A. Burnham, Appl. Phys. Lett. 63 (1993) 114.
[43] G.E.W. Schulze, M. Biermann, J. Mater. Sci. Lett. 12 (1993) 11.